Texture analysis based on the Hermite transform for image classification and segmentation

Alfonso Estudillo-Romero, Boris Escalante-Ramirez and Jesus Savage-Carmona

Universidad Nacional Autonoma de Mexico Fac. de Ingenieria, Edif. de Posgrado e Investigacion Ciudad Universitaria, C.P. 04510, Mexico, D.F., Mexico

ABSTRACT

Texture analysis has become an important task in image processing because it is used as a preprocessing stage in different research areas including medical image analysis, industrial inspection, segmentation of remote sensed imaginary, multimedia indexing and retrieval. In order to extract visual texture features a texture image analysis technique is presented based on the Hermite transform. Psychovisual evidence suggests that the Gaussian derivatives fit the receptive field profiles of mammalian visual systems. The Hermite transform describes locally basic texture features in terms of Gaussian derivatives. Multiresolution combined with several analysis orders provides detection of patterns that characterizes every texture class. The analysis of the local maximum energy direction and steering of the transformation coefficients increase the method robustness against the texture orientation. This method presents an advantage over classical filter bank design because in the latter a fixed number of orientations for the analysis has to be selected. During the training stage, a subset of the Hermite analysis filters is chosen in order to improve the inter-class separability, reduce dimensionality of the feature vectors and computational cost during the classification stage. We exhaustively evaluated the correct classification rate of real randomly selected training and testing texture subsets using several kinds of common used texture features. A comparison between different distance measurements is also presented. Results of the unsupervised real texture segmentation using this approach and comparison with previous approaches showed the benefits of our proposal.

Keywords: Hermite transform, steered Hermite transform, texture classification, texture segmentation, feature selection

1. INTRODUCTION

Description of images by its texture has an important role in many applications. Increasingly methods to browse, find and retrieve images on large databases are based on relevant content for the user such as the texture. Browsing medical images for diagnosis aid,[1] classification of the quality of a given process in industrial environments[23] and indexing of manuscripts[4] are some examples.

For texture analysis many techniques have emerged, such as gray-level co-occurrence matrices,[5] Markov random field models,[6] local binary patterns[7] and, filtered based methods including Gabor filters[8] and different wavelets types.[9,10] The Gabor filtering based technique has been widely used due to the fact that the Gabor functions are capable to model the receptive field profiles of simple cells of mammalian visual systems. Another reason is their optimal joint resolution in both the space and frequency domains.[11]

The Cartesian Hermite transform is a local decomposition technique that expands an image into orthogonal polynomials with respect to a Gaussian window.[12] One of the advantages of using the Hermite transform over other wavelet-based methods is that its analysis functions are similar to Gaussian derivatives. Psychovisual evidence supports the idea that the Gaussian derivatives fit the receptive field profiles of mammalian visual systems.[13]

Further author information: (Send correspondence to A.E.R.)
A.E.R.: e-mail: aestudillor@uxmcc2.iimas.unam.mx
B.E.R.: e-mail: boris@servidor.unam.mx
J.S.C.: e-mail: savage@servidor.unam.mx

Optics, Photonics, and Digital Technologies for Multimedia Applications II, edited by Peter Schelkens, Touradj Ebrahimi, Gabriel Cristóbal, Frédéric Truchetet, Pasi Saarikko,
Proc. of SPIE Vol. 8436, 843619 · © 2012 SPIE · CCC code: 0277-786X/12/$18 · doi: 10.1117/12.922658

Research has shown that the steered Hermite transform[14–16] is an efficient way to compactly describe image features into a smaller number of coefficients than the Cartesian Hermite transform. Moreover, since the steering direction depends on the local maximum energy, it is possible to obtain image descriptors invariant to the image orientation. This method presents an advantage over classical filter bank design because in the latter a fixed number of orientations for the analysis has to be selected.[4]

Previous works have proposed a Gabor-like Hermite model.[17] The Hermite transform has been tested in denoising and indexing experiments[4,18] using the Hermite analysis filters tuned at a fixed number of orientations. Others have used the steered Hermite transform for texture retrieval.[19] In this work we discuss some of the effects on classification performance of dimensionality reduction methods, the kinds of texture features and the distances that better classify textures.

An important issue when using filter-based methods to extract texture features is the filter bank parameter design. Common methods find an *optimal* filter bank design based on the spatial frequency coverage giving much importance to the orthogonality of the basis filters.[20] Orthogonality is required in the wavelet theory and there are two main reasons why it is important to consider it: one is to perform perfect reconstruction of the decomposition[21] and the other relies in the assumption that a minimal amount of overlapping, which means less redundant information, provides better discrimination rates.[22] Since texture feature extraction does not require image reconstruction it is possible to drop out the orthogonality requirements and to consider overlapping analysis functions. Recent research has also suggested that a certain amount of overlap between the frequency filter responses could improve classification.[23] However, keeping too much information has computational and storage drawbacks. Then, a strategy is required in order to select a set of filters that reduces the feature vector size, the computational costs and eventually improves texture discrimination.

Common feature and filter selection schemes include: selection of the filter frequencies that correspond to the principal spectral peaks of the texture,[8] based on the selection of the filtered image that best approximates a reconstruction function,[24] stochastic optimization[25] and genetic algorithms.[26] A disadvantage of the feature selection strategy in[27] is that this is performed after the classification stage by selecting the features that show the highest correct classification rate (CCR). The method employed in[28] and for dimensionality reduction of the feature vectors is based on principal components analysis (PCA). However, every principal component is a linear combination of the whole elements in the feature vector, this means that the number of filtering operations is not reduced during the classification stage. Moreover, after a PCA transformation the feature elements in the original feature space that provides better discrimination between texture classes remain unknown.[29]

In this paper we use the *augmented variance ratio* (AVR)[30] to obtain the most discriminant filter indexes from the training texture features and then use these filters to perform classification during the testing stage. We compare the CCRs as a function of the number of principal components (PCs) obtained from PCA and the number of features obtained from AVR.

Section 2 presents the Cartesian and steered Hermite transforms. Feature dimensionality reduction and filter selection for texture classification are presented in Sect. 3. Experimental setup and results for texture classification are detailed in Sect. 4. Segmentation results are shown in Sect. 5. Section 6 concludes this paper.

2. HERMITE TRANSFORM

For the one dimensional case, a polynomial transform $L_n(x)$ is a local decomposition technique in which an input signal $L(x)$ is localized through a window $V(x)$ and then expanded into orthogonal polynomials $G_n(x)$ at every window position:[12]

$$L_n(x_0) = \int_x L(x) G_n(x_0 - x) V_n^2(x_0 - x) dx \tag{1}$$

The Hermite transform arises when G_n are the Hermite polynomials $H_n(x)$, given by Rodrigues' formula:[31]

$$H_n(x) = (-1)^n e^{x^2} \frac{d^n e^{-x^2}}{dx^n}, \quad n = 0, 1, 2, \ldots \tag{2}$$

and the orthogonal window corresponds to a Gaussian window:

$$V(x) = \frac{1}{\sqrt{\sqrt{\pi}\sigma}} \cdot e^{-x^2/2\sigma^2} \tag{3}$$

From Eq. 1, the expansion coefficients $L_n(x)$ can be derived by convolution of the input signal $L(x)$ with the Hermite analysis functions $d_n(x)$. These are described in terms of the window and the Hermite polynomials as:

$$d_n(x) = \frac{(-1)^n}{\sqrt{2^n n!}} \cdot \frac{1}{\sigma\sqrt{\pi}} H_n\left(\frac{x}{\sigma}\right) e^{-x^2/\sigma^2} \tag{4}$$

Generalization of the Hermite analysis functions to two dimensions can be easily extended, since the analysis functions have the property of being both spatially separable and rotationally symmetric. We then can write the two dimensional analysis functions as:

$$d_{n-m,m}(x,y) = d_{n-m}(x)d_m(y) \tag{5}$$

where $n-m$ and m denote the analysis order in x and y direction respectively. As a result, we can expand a given input image $L(x,y)$ according to the 2D analysis function of Eq. 5 as:

$$L_{n-m,m}(x_0,y_0) = \int_x \int_y L(x,y) \cdot d_{n-m,m}(x_0-x, y_0-y)dxdy \tag{6}$$

for $n = 0, 1, \ldots, \infty$ and $m = 0, \ldots, n$. Figure 1 shows the Cartesian decomposition of the Hermite transform at one scale of analysis. From left to right and from top to bottom the analysis order increases in the x-direction and y-direction respectively.

A steerable filter is described as an arbitrary oriented filter synthesized from a linear combination of *basis filters*.[32] Since all Hermite analysis filters are polynomials times a radially symmetric window function, rotated versions of a filter of order n can be constructed by taking linear combinations of the original filters of order n. In this way, a more general expression of the original $L_{n-m,m}$ Cartesian Hermite coefficients can be written in terms of the orientation selectivity θ:[15]

$$L^{\theta}_{n-m,m}(x_0,y_0,\theta) = \sum_{k=0}^{n} L_{n-k,k}(x_0,y_0)\alpha_{n-k,k}(\theta) \tag{7}$$

which has been named the steered Hermite transform in.[14] The terms $\alpha_{n-m,m}(\theta)$ are the Cartesian angular functions of order n that provide such orientation selectivity and are defined as:

$$\alpha_{n-m,m}(\theta) = \sqrt{C^m_n}\cos^{n-m}(\theta)\sin^m(\theta) \tag{8}$$

where C corresponds to a binomial window which approximates the discrete Gaussian window.

The local energy can be written in terms of the steered Hermite coefficients as:

$$E_N = \sum_{n=0}^{N}\sum_{m=0}^{n}[L_{n-m,m}]^2 = \sum_{n=0}^{N}\sum_{m=0}^{n}[L^{\theta}_{n-m,m}]^2 \tag{9}$$

for all $N \geq 0$. In natural images, many of the image details that are of prime importance, such as edges and lines, can be locally described as one-dimensional patterns, that is, patterns that vary only in one direction (and are constant along the orthogonal direction). One may distinguish 1D local energy terms and 2D local energy terms. Thus, we can split local energy of (9) up to order N as:

$$E_N = [L_{0,0}]^2 + E^{1D}_N + E^{2D}_N \tag{10}$$

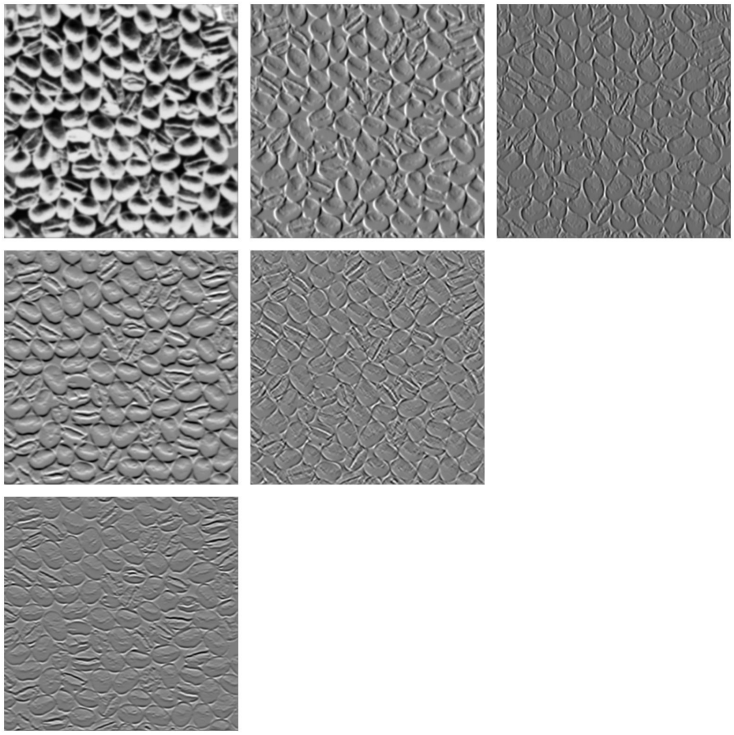

Figure 1. Cartesian Hermite decomposition at one scale of analysis. Input texture corresponds to a region from the Brodatz texture D74[33]

where $L_{0,0}$ represents the DC Hermite coefficient and

$$E_N^{1D} = \sum_{n=1}^{N} [L_{n,0}^{\theta}]^2 \tag{11}$$

$$E_N^{2D} = \sum_{n=1}^{N} \sum_{m=1}^{n} [L_{n-m,m}^{\theta}]^2 \tag{12}$$

In order to maximize detection of patterns we locally select θ as the angle between the horizontal and vertical Cartesian Hermite coefficients of first order. Energy compaction of the Cartesian Hermite coefficients as shown Fig. 1 can be efficiently achieved after steering such coefficients as it is shown in Fig. 2.

3. FEATURE DIMENSIONALITY REDUCTION AND FILTER SELECTION

We propose to extract texture features using an over-complete decomposition during the training stage. In order to select a subset of the *optimal* filters it is necessary to process each training texture with a full Hermite decomposition followed by a steering Hermite transformation. Then the features can be extracted from the steered coefficients. Our methodology was evaluated with several kinds of texture features found in the literature:

1. mean,

$$\mu = \frac{1}{H \times W} \sum_{w=1}^{W} \sum_{h=1}^{H} L_{n,0}^{\theta} \tag{13}$$

2. standard deviation,

$$\sigma = \sqrt{\frac{1}{(H \times W - 1)} \sum_{w=1}^{W} \sum_{h=1}^{H} [L_{n,0}^{\theta} - \mu]^2} \tag{14}$$

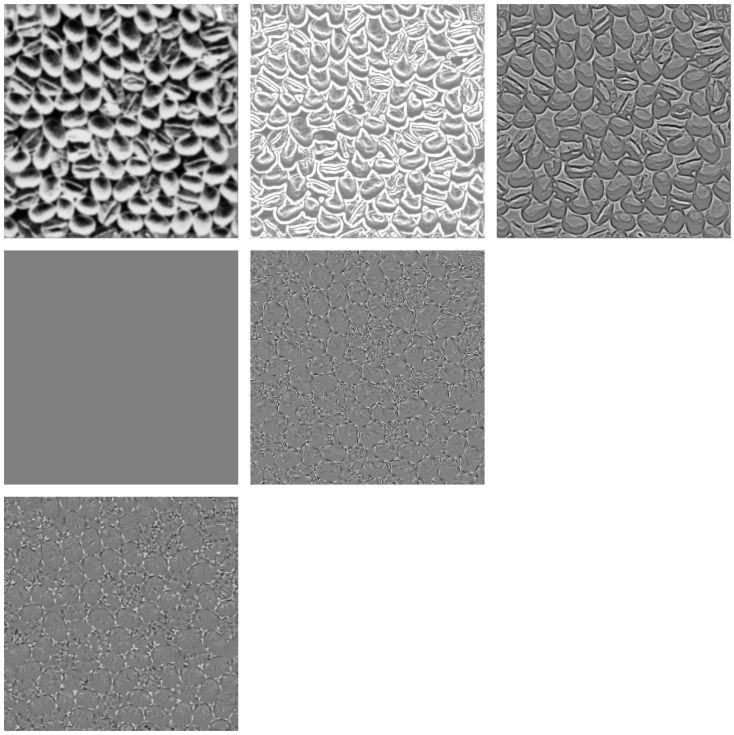

Figure 2. Steered Hermite decomposition for one scale of analysis. Input texture corresponds to a region from the Brodatz texture D74.[33] Most visual information has been compacted on the first row as 1D patterns

3. and four energy features

$$E_0 = \sum_{w=1}^{W} \sum_{h=1}^{H} [L^{\theta}_{n,0}]^2 \tag{15}$$

$$E_1 = \frac{E_0}{H \times W} \tag{16}$$

$$E_2 = \frac{1}{H \times W} \sum_{w=1}^{W} \sum_{h=1}^{H} |L^{\theta}_{n,0}| \tag{17}$$

$$E_3 = \frac{1}{H \times W} \sum_{w=1}^{W} \sum_{h=1}^{H} \sqrt{|L^{\theta}_{n,0}|} \tag{18}$$

where H and W are the dimensions of the steered Hermite coefficients.

Different kinds of feature vectors are formed by concatenating the texture features extracted from the steered Hermite transform at every scale of analysis s and for every analysis order n, where $1 \leq s \leq S$ and $1 \leq n \leq N$ with S and N being the maximum scale and analysis order respectively. The i-th vector for every one of the texture features can be written as:

$$\mathbf{v}_i = [v_{i_1}^{(1)}, v_{i_2}^{(1)}, \ldots, v_{i_N}^{(1)}, v_{i_1}^{(2)}, \ldots, v_{i_N}^{(S)}] \tag{19}$$

Note that we can simplify Eq. 19 by using the index j such that $1 \leq j \leq S \times N$ as:

$$\mathbf{v}_i = [v_{i,1}, \ldots, v_{i,j}] \tag{20}$$

Once all the features are obtained from the training textures set, these are arranged in a feature matrix as shown in Eq.21, where q and r represent the number of measures or vectors and the number of elements in each vector respectively.

$$\mathbf{F_V} = \begin{bmatrix} v_{1,1} & v_{1,2} & \dots & v_{1,r} \\ v_{2,1} & v_{2,2} & \dots & v_{2,r} \\ \vdots & \vdots & \vdots & \vdots \\ v_{q,1} & v_{q,2} & \dots & v_{q,r} \end{bmatrix} \tag{21}$$

3.1 PCA

We perform PCA over the training features matrix in order to reduce dimensionality and we compare the CCR after PCA against the CCR obtained after the filter selection strategy using AVR. Our hypothesis is that the minimum number of PCs that better classify textures without filter selection should converge to the case when this filter selection procedure is employed with the advantage that a subset of the *optimal* steered Hermite coefficients should be known prior testing. Moreover, it is expected that filter selection could improve classification accuracy.

In order to transform each feature vector defined in the set $\mathbf{V}$ into another feature vector defined in the new set $\mathbf{Y}$ we look for a transformation $\mathbf{W}$, such that the covariance matrix of the elements in $\mathbf{Y}$ is diagonal. The transformation is linear and it is defined as:

$$\mathbf{F_Y} = \mathbf{F_V}\mathbf{W}^T \tag{22}$$

where $\mathbf{W}^T$ is the matrix of eigenvectors we search for. The new set of features (projected training features) is obtained by simple multiplication of the original training features with the eigenmatrix $\mathbf{W}^T$. The same procedure is performed in order to obtain the projected testing features.

3.2 Augmented Variance Ratio (AVR)

The *Augmented Variance Ratio* (AVR) proposed in[30] has been shown to provide a quantitative basis to separate non-discriminative features before feature subset selection. The AVR is defined as:

$$AVR(F) = \frac{Var(S_F)}{\frac{1}{C}\sum_{i=1..C} \frac{Var_i(S_F)}{min_{i \neq j}(|M_i(S_F) - M_j(S_F)|)}} \tag{23}$$

where $Var(S_F)$ is the cross-class variance of feature F, $Var_i(S_F)$ and $M_i(S_F)$ are the within-class variance and mean of the feature F for class i out of C distinct classes. Similar to Fisher criterion,[34] AVR represents the ratio of cross-class variance of the feature over within-class variance, with added penalty to features that have close inter-class means.

By ranking in descendant order the indexes of the feature vectors with high AVR it is possible to know the indexes of the filters that were used to obtain such features. With these indexes, sorted in descendant order according to the AVR values, filter selection to extract testing texture features is a straightforward procedure.

4. TEXTURE CLASSIFICATION

We exhaustively evaluated our proposal by randomly selecting different training and testing sets 80 times. Training sets were formed from 20 texture images each time.

4.1 Dataset

The method was evaluated with a subset of real and natural rotated texture images from the Outex database (available on-line at http://www.outex.oulu.fi). The texture classes that were used are coded in the Outex database as: *canvas001*, *canvas002*, *canvas003*, *canvas005*, *canvas006*, *canvas009*, *canvas011*, *canvas021*, *canvas022*, *canvas023*, *canvas025*, *canvas026*, *canvas031*, *canvas032*, *canvas033*, *canvas035*, *canvas038*, *canvas039*, *tile005*, *tile006*, *carpet002*, *carpet004*, *carpet005* and *carpet009*.

The texture images were acquired with incandescent illumination, coded as "inca" in the Outex database, at 100 dpi spatial resolution and nine rotation angles (0°, 5°, 10°, 15°, 30°, 45°, 60°, 75° and 90°). The 24-bit RGB images were transformed into eight bit intensity images using:

$$I = 0.299R + 0.587G + 0.114B \tag{24}$$

The evaluation set was formed with 20 non-overlapping texture samples of size 128×128 pixels selected from each intensity image class from 0° to 90° by centering a sampling grid of 5×4 so that equal number of pixels were left over on each side of the sampling grid. As a result $24 \times 20 \times 9 = 4320$ texture images were used.

4.2 Classification

We evaluated classification accuracy based on the k-NN classifier using two distance measurements and the classifier using the Mahalanobis distance. The k-NN classifier consists of assigning a class label to a sample vector based on the mode of its k nearest neighbors vectors. Given two feature vectors $\mathbf{v}_1$ and $\mathbf{v}_2$ of r features, then the Euclidean distance is defined as:

$$d_E(\mathbf{v}_1, \mathbf{v}_2) = \sqrt{\sum_{j=1}^{r} (v_{1,j} - v_{2,j})^2} \tag{25}$$

and the Canberra distance as:

$$d_C(\mathbf{v}_1, \mathbf{v}_2) = \sum_{j=1}^{r} \frac{|v_{1,j} - v_{2,j}|}{|v_{1,j}| + |v_{2,j}|} \tag{26}$$

The Mahalanobis classifier assigns a class label to a sample vector by taking the minimum distance from all the computed distances between each mean class vector $\bar{\mathbf{x}}$ and the sample vector by also considering the covariance feature matrix. The Mahalanobis distance of a sample vector $\mathbf{v}_1$ to a class $\mathbf{F_C}$ is defined as:

$$d_M(\mathbf{v}_1, \mathbf{C}) = \sqrt{(\mathbf{v}_1 - \bar{\mathbf{c}}) \Sigma_{\mathbf{C}}^{-1} (\mathbf{v}_1 - \bar{\mathbf{c}})^T} \tag{27}$$

where $\mathbf{F_C}$ is the feature matrix for class $\mathbf{C}$, $\bar{\mathbf{c}}$ its mean vector and $\Sigma_{\mathbf{C}}^{-1}$ the inverse covariance for the class if it exists. Classification accuracy is measured by computing the CCR defined as:

$$\text{CCR} = \frac{N_c}{N_{Te}} \tag{28}$$

where N_c is the number of testing images that were correctly classified and N_{Te} is the total number of testing images.

4.3 Classification results

The 14 feature indexes that were selected using the AVR dimensionality reduction and filter selection method are shown in Fig. 3. From left to right in every plot, the bars represent the AVR values of the feature index in the training feature matrix. The four groups of bars represent each one of the $S = 4$ scale of analysis. The eight bars of each group represent each one the order (up to order $N = 8$) of the steered Hermite coefficient that contributed with a feature.

Figure 4 shows the average CCRs obtained with the three distances and for all texture features respectively. These evaluations show the CCRs as a function of the number of PCs (PCA, first row) and the number of feature indexes (AVR, second row). In most cases it is common to see that the AVR. The Mahalanobis distance showed better CCRs for the first number of PCs or feature indexes. The feature σ showed the worst CCRs.

Table 1 summarizes the CCR performances and compares PCA with AVR by using only 9 PCs or texture feature indexes for all kinds of texture features and the different distance measurements that were used. Depending on the kind of texture feature and the used distance, AVR showed similar and in some cases improved the CCRs compared to the CCRs obtained by means of PCA. For all cases using either PCA or AVR, the Mahalanobis distance showed better CCRs, especially if the feature vector was small. Using 9 feature indexes and the Mahalanobis distance the features that offered better CCRs were μ, E_2, E_3.

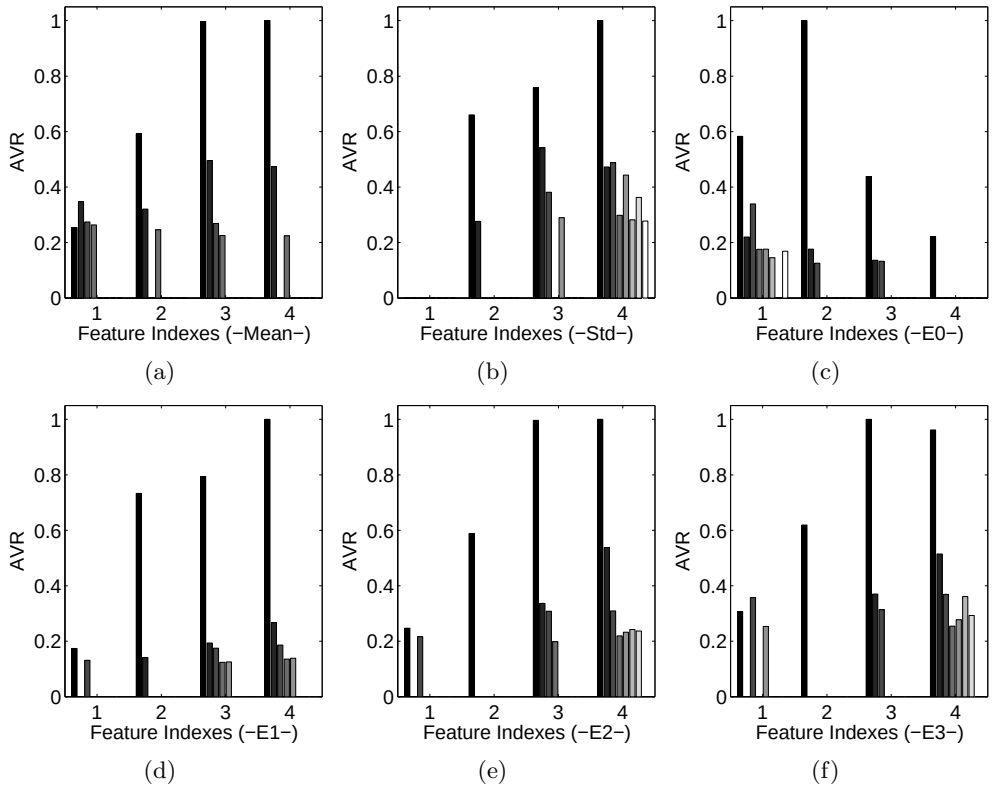

Figure 3. Feature indexes and their AVR values for: a)μ, b)σ, c) E_0, d) E_1, e) E_2, f) E_3 for dataset II.

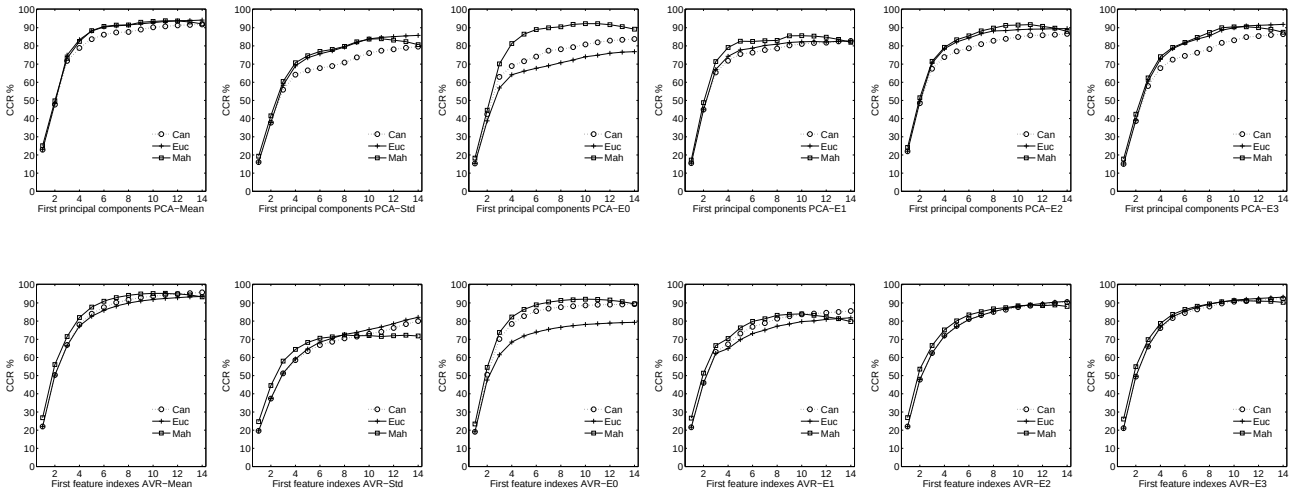

Figure 4. Comparison of CCRs obtained with the Canberra, Euclidean and Mahalanobis distances for texture classification. From the top to bottom each row corresponds to the CCRs obtained with PCA and AVR respectively and, from left to right each column corresponds to the features μ, σ, E_0, E_1, E_2, and E_3 respectively.

Table 1. Comparison of CCRs (%) for texture classification

Feature	PCA	AVR
μCan	89.02 @ 9	**92.94 @ 9**
μEuc	**92.13 @ 9**	91.11 @ 9
μMah	93.03 @ 9	**94.95 @ 9**
σCan	**73.66 @ 9**	71.50 @ 9
σEuc	**81.84 @ 9**	73.81 @ 9
σMah	**82.25 @ 9**	71.96 @ 9
E_0Can	79.28 @ 9	**88.25 @ 9**
E_0Euc	72.23 @ 9	**77.53 @ 9**
E_0Mah	**91.86 @ 9**	91.74 @ 9
E_1Can	80.25 @ 9	**82.62 @ 9**
E_1Euc	**81.92 @ 9**	78.41 @ 9
E_1Mah	**85.54 @ 9**	83.75 @ 9
E_2Can	83.86 @ 9	**86.28 @ 9**
E_2Euc	**88.45 @ 9**	86.68 @ 9
E_2Mah	**91.31** @ 9	87.41 @ 9
E_3Can	81.65 @ 9	**89.70 @ 9**
E_3Euc	88.65 @ 9	**90.65 @ 9**
E_3Mah	90.01 @ 9	**90.67 @ 9**

5. TEXTURE SEGMENTATION

For texture segmentation we first processed the input texture with the Cartesian Hermite transform and then performed steering of the Cartesian Hermite coefficients. In these experiments we used 4 scales of analysis and Cartesian Hermite coefficients up to order 4. Thus 16 steered Hermite coefficients or feature images were obtained. In order to test our proposal we followed a similar methodology presented in.[24] A non-linearity was applied to each steered Hermite coefficient with $\alpha = 0.25$:

$$\psi(t) = \tanh(\alpha t) = \frac{1 - e^{-2\alpha t}}{1 + e^{-2\alpha t}} \tag{29}$$

The non-linearity of the steered Hermite coefficients was followed by a smoothing post-processing task using a Gaussian window. In order to classify texture regions we used the K-means clustering algorithm. Figures 5a and 6a show the original images containing 3 and 5 texture classes respectively that were used to test the correct segmentation accuracy (CSR) defined as:

$$\text{CSR} = \frac{N_c\text{pix}}{N\text{pix}} \tag{30}$$

where $N_c$pix is the number of pixels that were correctly segmented and Npix is the total number of pixels in the image. The feature vectors were formed from the 16 steered Hermite coefficients plus the spatial coordinates of the pixels.

5.1 Segmentation results

Figures 5c and 6c show segmentation results for images containing 3 and 5 texture classes respectively. Figures 5b and 6b show the ground truth of the segmentation. The CSR for the image containing 3 texture classes was 98.30% whereas the image containing 5 texture classes was 94.11%.

(a) (b) (c)

Figure 5. Texture segmentation. a) original image, b) ground truth segmentation of three classes and c) segmentation result

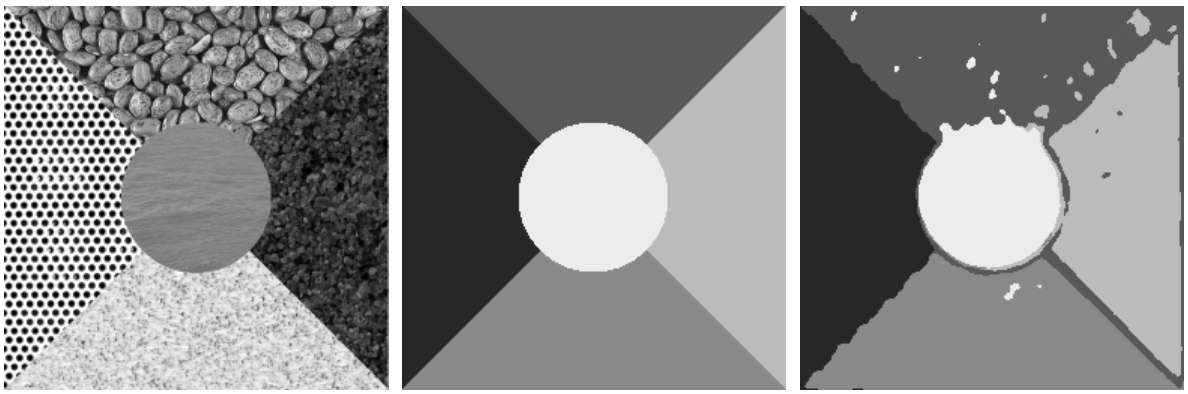

(a) (b) (c)

Figure 6. Texture segmentation. a) original image, b) ground truth segmentation of five classes and c) segmentation result

6. CONCLUSIONS

Computation of CCRs using natural rotated textures from the Outex database showed that the features extracted from the steered Hermite transform are robust against the texture orientation. The AVR feature dimensionality reduction and filter selection strategy showed superior CCRs compared to those obtained after a simple feature dimensionality reduction using PCA. An interesting finding was that high CCRs were achieved by using only a small set of feature elements. It was not possible to establish which distance performed the best CCRs. Nevertheless, we noticed that in many cases the Mahalanobis distance was superior to the Canberra and Euclidean distances, especially for small feature vectors.

Segmentation results showed that the coefficients obtained by means of the steered Hermite transform are also suitable for texture segmentation. As for the classification problem, only a small number of steered coefficients was required. This is an advantage over other filter-based segmentation techniques.

ACKNOWLEDGMENTS

This work was supported by UNAM grants PAPIIT IN113611 and IXTLI IX100610. Doctoral scholarship supported by CONACyT grant 173482.

REFERENCES

[1] Quellec, G., Lamard, M., Cazuguel, G., Cochener, B., and Roux, C., "Wavelet optimization for content-based image retrieval in medical databases," *Medical Image Analysis* **14**(2), 227–241 (2010).

[2] Arivazhagan, S., Ganesan, L., and Bama, S., "Fault segmentation in fabric images using Gabor wavelet transform," *Machine Vision and Applications* **16**(6), 356–363 (2006).
[3] Liu, L., Ngadi, M., Prasher, S., and Gariépy, C., "Categorization of pork quality using gabor filter-based hyperspectral imaging technology," *Journal of Food Engineering* **99**(3), 284–293 (2010).
[4] Bres, S., Eglin, V., and Rivero, C., "Handwriting documents denoising and indexing using hermite transform," in [*Pattern Recognition and Data Mining*], *LNCS* **3686**, 664–673 (2005).
[5] Haralick, R., "Statistical and structural approaches to texture," *Proceedings of the IEEE* **67**(5), 786–804 (1979).
[6] Cross, G. R. and Jain, A. K., "Markov random field texture models," *IEEE Trans. PAMI* **5**(1), 25–39 (1983).
[7] Ojala, T., Pietikäinen, M., and Mäenpää, T., "Multiresolution gray-scale and rotation invariant texture classification with local binary patterns," *IEEE Trans. PAMI* **24**(7), 971–987 (2002).
[8] Bovik, A. C., Clark, M., and Geisler, W. S., "Multichannel texture analysis using localized spatial filters," *IEEE Trans. PAMI* **12**(1), 55–73 (1990).
[9] Pun, C.-M. and Lee, M.-C., "Log-polar wavelet energy signatures for rotation and scale invariant texture classification," *IEEE Trans. PAMI* **25**(5), 590–603 (2003).
[10] Manthalkar, R., Biswas, P. K., and Chatterji, B. N., "Rotation and scale invariant texture features using discrete wavelet packet transform," *Pattern Recognition Letters* **24**(14), 2455–2462 (2003).
[11] Daugman, J. G., "Uncertainty relation for resolution in space, spatialfrequency, and orientation optimized by two-dimensional visual cortical filters," *J. Opt. Soc. Am.* **A 2**(7), 1160–1169 (1985).
[12] Martens, J.-B., "The hermite transform-theory," *IEEE Transactions on Acoustics, Speech and Signal Processing* **38**(9), 1595–1606 (1990).
[13] Young, R. A., "Orthogonal basis functions for form vision derived from eigenvector analysis," in [*ARVO Abstracts*], *ARVO Abstracts* , 22, Association for Research in Vision and Ophthalmology, Abstract, Sarasota, FL (1978).
[14] van Dijk, A. M. and Martens, J.-B., "Image representation and compression with steered hermite transforms," *Signal Processing* **56**(1), 1–16 (1997).
[15] Silvan-Cardenas, J. and Escalante-Ramirez, B., "The multiscale hermite transform for local orientation analysis," *IEEE Transactions on Image Processing* **15**(5), 1236–1253 (2006).
[16] Martens, J.-B., "The Hermite transform: a survey," *EURASIP Journal of Applied Signal Processing* **26145**, 1110–8657 (2006).
[17] Rivero-Moreno, C. J. and Bres, S., "Conditions of similarity between hermite and gabor filters as models of the human visual system," in [*Computer Analysis of Images and Patterns*], *LNCS* **2756**, 762–769 (2003).
[18] Eglin, V., Bres, S., and Rivero, C., "Hermite and gabor transforms for noise reduction and handwriting classification in ancient manuscripts," *International Journal on Document Analysis and Recognition* **9**, 101–122 (2007).
[19] Estudillo-Romero, A. and Escalante-Ramirez, B., "Advances in rotation-invariant texture analysis," in [*Progress in Pattern Recognition, Image Analysis, Computer Vision, and Applications*], *LNCS* **5856**, 145–152 (2009).
[20] Haley, G. and Manjunath, B., "Rotation-invariant texture classification using a complete space-frequency model," *IEEE Transactions on Image Processing* **8**(2), 255–269 (1999).
[21] Lee, T. S., "Image representation using 2D Gabor wavelets," *IEEE Trans. PAMI* **18**(10), 959–971 (1996).
[22] Manjunath, B. S. and Ma, W. Y., "Texture features for browsing and retrieval of image data," *IEEE Trans. PAMI* **18**(8), 837–842 (1996).
[23] Bianconi, F. and Fernandez, A., "Evaluation of the effects of Gabor filter parameters on texture classification," *Pattern Recognition* **40**(12), 3325–3335 (2007).
[24] Jain, A. K. and Farrokhnia, F., "Unsupervised texture segmentation using Gabor filters," *IEEE International Conference on Systems, Man and Cybernetics* , 14–19 (1990).
[25] Tsai, D.-M., Wu, S.-K., and Chen, M.-C., "Optimal Gabor filter design for texture segmentation using stochastic optimization," *Image and Vision Computing* **19**(5), 299–316 (2001).

[26] Li, F. and Xu, K., "Optimal gabor kernel's scale and orientation selection for face classification," *Optics & Laser Technology* **39**(4), 852–857 (2007).
[27] Chu, X. and Chan, K., "Rotation and scale invariant texture analysis with tunable gabor filter banks," in [*Advances in Image and Video Technology*], *LNCS* **5414**, 83–93 (2009).
[28] Celik, T. and Tjahjadi, T., "Bayesian texture classification and retrieval based on multiscale feature vector," *Pattern Recognition Letters* **32**(2), 159–167 (2011).
[29] Estudillo-Romero, A. and Escalante-Ramirez, B., "Classification of low level visual texture features based on the hermite transform," in [*Signal-Image Technology and Internet-Based Systems (SITIS)*], 461–467 (2011).
[30] Liu, Y., Teverovskiy, L., Carmichael, O., Kikinis, R., Shenton, M., Carter, C. S., Stenger, V. A., Davis, S., Aizenstein, H., Becker, J. T., Lopez, O. L., and Meltzer, C. C., "Discriminative MR image feature analysis for automatic schizophrenia and alzheimers disease classification," in [*Medical Image Computing and Computer-Assisted Intervention – MICCAI 2004*], *LNCS* **3216**, 393–401 (2004).
[31] Abramowitz, M. and Stegun, I., [*Handbook of Mathematical Functions*], Dover (1965).
[32] Freeman, W. and Adelson, E., "The design and use of steerable filters," *IEEE Trans. PAMI* **13**(9), 891–906 (1991).
[33] Brodatz, P., [*Texture: a photographic album for artists and designers*], New York: Dover (1966).
[34] Fisher, R. A., "The use of multiple measurements in taxonomic problems," *Annals of Human Genetics* (7), 179–188 (1936).